

**FIRST-PRINCIPLES STUDY OF THE  
STRUCTURAL, STABILITY AND ELECTRONIC  
PROPERTIES OF SMALL ALUMINUM-  
TITANIUM-NICKEL CLUSTERS**

**KOH PIN WAI**

**UNIVERSITI SAINS MALAYSIA**

**2021**

**FIRST-PRINCIPLES STUDY OF THE  
STRUCTURAL, STABILITY AND ELECTRONIC  
PROPERTIES OF SMALL ALUMINUM-  
TITANIUM-NICKEL CLUSTERS**

by

**KOH PIN WAI**

**Thesis submitted in fulfilment of the requirements  
for the degree of  
Doctor of Philosophy**

**April 2021**

## ACKNOWLEDGEMENT

The completion of my Ph. D. study is the result of contributions from various parties. First of all, I wish to express my sincerely gratitude to my supervisor, Dr. Yoon Tiem Leong, who always providing technical support and valuable idea throughout my study. I am thankful to my mentor, Dr. Lim Thong Leng from Multimedia University, also shared his crucial advices on the technical details in DFT. Their motivation and valuable ideas, as well as the tireless commitment in this research, are utmost helpful, especially in leading my learning path as a researcher. For their help and concerns in my studies, I am greatly indebted to both of them. In addition, I am grateful to Prof. Lai San Kiong and Dr. Yen Tsung Wen, from National Central University of Taiwan, for organizing the student exchange program and academic support on Modified Basin Hopping.

The financial support from Ministry of Higher Education in term of MyPhd scholarship in covering my tuition fees is acknowledged. Also, I would like to thank the School of Physics to provide the financial support for me to attend the 9th Asian Consortium on Computational Materials Science held.

For the immediate colleagues from the theoretical and computational group, I am grateful to them for the guidance with the valuable technical advice on installation and maintenance of software and hardware. They are Goh Eng Seng, Lian Ming Huei, Robin Chang Yee Hui, MinTjun Kit, Ng Wei Chun, Soon Yee Yeen and Ong Yee Pin.

Last but not least, I am grateful for my family who supports me in all aspects. They understand and respect my decisions during the completion of my project, and thesis. The hard works and sacrifices they have made encourage me even more to succeed both in life and in academic.

## TABLE OF CONTENTS

<b>ACKNOWLEDGEMENT</b> .....	<b>ii</b>
<b>TABLE OF CONTENTS</b> .....	<b>iii</b>
<b>LIST OF TABLES</b> .....	<b>vii</b>
<b>LIST OF FIGURES</b> .....	<b>xi</b>
<b>LIST OF SYMBOLS</b> .....	<b>xv</b>
<b>LIST OF ABBREVIATIONS</b> .....	<b>xvii</b>
<b>LIST OF APPENDICES</b> .....	<b>xix</b>
<b>ABSTRAK</b> .....	<b>xx</b>
<b>ABSTRACT</b> .....	<b>xxiv</b>
<b>CHAPTER 1 INTRODUCTION</b> .....	<b>1</b>
1.1 Motivation .....	2
1.2 Problem statement .....	4
1.3 Objectives of study .....	5
1.4 Background studies of Al-Ti-Ni nanoclusters.....	6
1.5 Thesis outline .....	10
<b>CHAPTER 2 LITERATURE REVIEW</b> .....	<b>12</b>
2.1 Computational simulation techniques on nanoclusters .....	12
2.2 Density functional theory .....	17
2.2.1 The Schrödinger Equation .....	17
2.2.2 Electron density.....	20
2.2.3 Hohenberg-Kohn theorem.....	22
2.2.4 Kohn-Sham formalism.....	25
2.2.5 Exchange-correlation functional .....	30
Local density approximation (LDA) .....	30
Generalized gradient approximation (GGA) .....	32

	Hybrid - Generalized gradient approximation (Hybrid - GGA).....	33
2.2.6	Basis sets .....	34
2.3	Searching for the ground state structure of an atomic cluster .....	36
<b>CHAPTER 3 METHODOLOGY .....</b>		<b>42</b>
3.1	Optimization techniques.....	42
3.1.1	Basin hopping .....	43
3.1.2	Genetic Algorithm.....	44
3.2	PTMBHGA+G09 (pg9).....	45
3.3	Two-stage global search algorithm for the lowest energy structure of a ternary cluster at the DFT level .....	48
3.3.1	First stage: PES scanning for the Al-Ti-Ni clusters.....	50
3.3.2	Second stage: Ground-state structure for the Al-Ti-Ni clusters.....	51
3.4	Spin multiplicity and contamination issue .....	55
3.5	Reliability of the B3LYP exchange-correlation functional in DFT.....	59
3.6	Comparison with recent experimental results .....	62
3.7	Computation cost and the choice of optimum basis set in the two-stage search algorithm .....	63
<b>CHAPTER 4 STRUCTURAL AND STABILITY OF ALUMINIUM-TITANIUM-NICKEL <math>Al_xTi_yNi_z</math> (<math>x + y + z = 4, 5</math> &amp; <math>6</math>) CLUSTERS.. .....</b>		<b>68</b>
4.1	Structural Properties .....	68
4.1.1	Structure properties of four atoms ternary $Al_xTi_yNi_z$ clusters.....	69
4.1.2	Structure properties of five atoms ternary $Al_xTi_yNi_z$ clusters .....	75
4.1.3	Structure properties of six atoms ternary $Al_xTi_yNi_z$ clusters.....	78
4.2	Cluster Stability: binding energy per atom ( <b><math>E_b</math></b> ), excess energy ( <b><math>E_{exc}</math></b> ) and the second difference energy ( <b><math>\Delta E</math></b> ).....	82
4.2.1	Stability of four-atom ternary $Al_xTi_yNi_z$ clusters .....	83
4.2.2	Stability of five-atom ternary $Al_xTi_yNi_z$ clusters.....	87
4.2.3	Stability of six-atom ternary $Al_xTi_yNi_z$ clusters .....	90

**CHAPTER 5 CHEMICAL ORDER AND ELECTRONIC PROPERTIES OF  
ALUMINIUM-TITANIUM-NICKEL  $Al_xTi_yNi_z$  ( $x + y + z = 4, 5$   
& 6) CLUSTERS ..... 95**

5.1	Chemical Order ( $\sigma$ ) .....	95
5.1.1	Chemical order of four atoms ternary $Al_xTi_yNi_z$ clusters.....	96
5.1.2	Chemical order of five atoms ternary $Al_xTi_yNi_z$ clusters .....	96
5.1.3	Chemical order of six atoms ternary $Al_xTi_yNi_z$ clusters.....	98
5.2	Electronic Properties: ionization potential (IP), electron affinity (EA), Global hardness ( $\eta$ ), Mulliken electronegativity ( $\xi$ ) and HOMO-LUMO energy gaps ( <b>E<sub>gap</sub></b> ).....	99
5.2.1	Electronics properties of four atoms ternary $Al_xTi_yNi_z$ clusters...	100
5.2.2	Electronics properties of five atoms ternary $Al_xTi_yNi_z$ clusters ...	105
5.2.3	Electronics properties of six atoms ternary $Al_xTi_yNi_z$ clusters.....	109
5.2.4	HOMO-LUMO energy gap calculations for six-atom open-shell ternary $Al_xTi_yNi_z$ clusters with restricted open-shell calculations	115

**CHAPTER 6 CONCLUSION ..... 119**

6.1	Conclusion .....	119
6.2	Recommendations for Future Research .....	122

**REFERENCES..... 125**

**APPENDICES**

**LIST OF PUBLICATIONS**

## LIST OF TABLES

	<b>Page</b>
Table 2.1	Different Types of Gaussian Basis Sets .....35
Table 3.1	Calculated spin eigenvalues for different spin states of B3LYP and ROB3LYP for six-atom Al-Ti-Ni clusters .....57
Table 3.2	Comparison of the binding energy of selected mono-atom type clusters between the present and published works .....60
Table 3.3	Computational time for Ni <sub>6</sub> , Ti <sub>2</sub> Ni <sub>4</sub> , Al <sub>2</sub> Ti <sub>2</sub> , Al <sub>2</sub> Ti <sub>2</sub> Ni <sub>2</sub> and Al <sub>4</sub> TiNi clusters generated using SVWN XC functional with different basis sets STO3G, 3-21G and 6-31G in the first of the two-stage calculation. ....65
Table 3.4	Lowest-energy LLS for Ni <sub>6</sub> , Ti <sub>2</sub> Ni <sub>4</sub> , Al <sub>2</sub> Ti <sub>2</sub> , Al <sub>2</sub> Ti <sub>2</sub> Ni <sub>2</sub> and Al <sub>4</sub> TiNi clusters generated in the first of the two-stage calculation using SVWN XC functional with basis sets STO-3G and 3-21G. The red atoms represent aluminium, blue atoms represent titanium and green atoms represent nickel. ....65
Table 3.5	Computational time for Ni <sub>6</sub> , Ti <sub>2</sub> Ni <sub>4</sub> , Al <sub>2</sub> Ti <sub>2</sub> , Al <sub>2</sub> Ti <sub>2</sub> Ni <sub>2</sub> and Al <sub>4</sub> TiNi clusters using B3LYP XC functional with basis set 6-311G* in the second of the two-stage calculation. ....66
Table 4.1	Structures of the four atoms Al-Ti-Ni cluster are showed. Numbers in the 1st, 3rd and 5th column indicate the number of Al, Ti and Ni atoms in each cluster. ....71
Table 4.2	Structures of the five atoms Al-Ti-Ni cluster are showed. Numbers in the 1st, 3rd and 5th column indicate the number of Al, Ti and Ni atoms in each cluster. ....75
Table 4.3	Structures of the six atoms Al-Ti-Ni cluster are showed. Numbers in the 1st, 3rd and 5th column indicate the number of Al, Ti and Ni atoms in each cluster. ....80

Table 4.4	Properties of $Al_xTi_yNi_z$ clusters with $x + y + z = 4$ . Numbers in the first column indicate the number of Al, Ti and Ni atoms in each cluster. The average interatomic distances (in Å), binding energy per atom ( $E_b$ in eV), excess energy ( $E_{exc}$ in eV), second order difference energy ( $\Delta E$ in eV), and HOMO-LUMO energy gaps ( $E_{gap}$ in eV) are presented in the table.....86
Table 4.5	Properties of $Al_xTi_yNi_z$ clusters with $x + y + z = 5$ . Numbers in the first column indicate the number of Al, Ti and Ni atoms in each cluster. The average interatomic distances (in Å), binding energy per atom ( $E_b$ in eV), excess energy ( $E_{exc}$ in eV), second order difference energy ( $\Delta E$ in eV), and HOMO-LUMO energy gaps ( $E_{gap}$ in eV) are presented in the table.....89
Table 4.6	Properties of $Al_xTi_yNi_z$ clusters with $x + y + z = 6$ . Numbers in the first column indicate the number of Al, Ti and Ni atoms in each cluster. The average interatomic distances (in Å), binding energy per atom ( $E_b$ in eV), excess energy ( $E_{exc}$ in eV), second order difference energy ( $\Delta E$ in eV), and HOMO-LUMO energy gaps ( $E_{gap}$ in eV) are presented in the table.....93
Table 5.1	Properties of $Al_xTi_yNi_z$ clusters with $x + y + z = 4$ . Numbers in the first column indicate the number of Al, Ti and Ni atoms in each cluster. The number of nearest neighbor pairs (the order is Al-Al, Ti-Ti, Ni-Ni, Al-Ni, Al-Ti and Ti-Ni, respectively), chemical order ( $\sigma$ ), ionization potential (IP in eV), electron affinity (EA in eV), global hardness ( $\eta$ in eV) and Mulliken electronegativity ( $\xi$ in eV) are presented in the table..... 104
Table 5.2	Properties of $Al_xTi_yNi_z$ clusters with $x + y + z = 5$ . Numbers in the first column indicate the number of Al, Ti and Ni atoms in each cluster. The number of nearest neighbor pairs (in sequence of Al-Al, Ti-Ti, Ni-Ni, Al-Ni, Al-Ti and Ti-Ni), chemical order ( $\sigma$ ), ionization potential (IP), electron affinity (EA), global hardness ( $\eta$ ) and Mulliken electronegativity ( $\xi$ ) are presented in the table..... 109



Table 5.3	Properties of the $\text{Al}_x\text{Ti}_y\text{Ni}_z$ clusters with $x + y + z = 6$ . Numbers in the first column indicate the number of Al, Ti and Ni atoms in each cluster. The number of nearest-neighbour pairs (in a sequence of Al-Al, Ti-Ti, Ni-Ni, Al-Ni, Al-Ti and Ti-Ni), chemical order ( $\sigma$ ), ionization potential (IP), electron affinity (EA), global hardness ( $\eta$ ) and Mulliken electronegativity ( $\xi$ ) are presented in the table. There is no unit for $\sigma$ and the unit of IP, EA, $\eta$ and $\xi$ is electron-volt (eV).....	114
Table 5.4	Comparison of the total energy of the $\text{Al}_x\text{Ti}_y\text{Ni}_z$ clusters with $x + y + z = 6$ that calculated by using UB3LYP and ROB3LYP XC functionals with the same basis sets 6-311G*. The unit of total energy in the 3 <sup>rd</sup> and 4 <sup>th</sup> column is in the unit of electron-volt (eV). .....	116
Table 5.5	Comparison of the HOMO-LUMO energy gap $E_{\text{gap}}$ (with multiplicity $M = 1$ or $2$ ) and $E_{\text{gap}}'$ (with actual multiplicity $M'$ ) of the $\text{Al}_x\text{Ti}_y\text{Ni}_z$ clusters with $x + y + z = 6$ . The unit of $E_{\text{gap}}$ and $E_{\text{gap}}'$ are in the unit of electron-volt (eV)......	117
Table A.1	Properties of $\text{Al}_x\text{Ti}_y\text{Ni}_z$ clusters with $x + y + z = 6$ . Numbers in the first column indicate the number of Al, Ti and Ni atoms in each cluster. $M$ refers to multiplicity, $E_T$ total energy, $E_{T+ZPE}$ summation of total energy and zero-point energy, $\langle\alpha\rangle$ static mean polarizability and $\langle\alpha\rangle / N$ mean polarizability. The asterisk (*) in the column $E_T$ indicates lowest energy. Cluster compositions with double asterisk (**) are that with lowest energy states occurring at the smallest multiplicity (i.e. $M$ equal either 1 or 2)......	140
Table A.2	Comparison of the geometric structures and average interatomic distances at two multiplicities. Cluster compositions with double asterisk (**) are that with lowest energy states occurring at the smallest multiplicity (i.e. $M$ equal either 1 or 2)......	144
Table B.3	Comparison of the geometric structures of $\text{Ni}_4$ , $\text{Ni}_5$ and $\text{Ni}_6$ with multiplicity $M = 1$ using molecular dynamic and density functional theory approaches. ....	147

Table C.4	Left: ground-state structures obtained in experiment (i) using 6-311G*; Right: ground-state structures obtained in experiment (ii) using LANL2DZ. ....	150
-----------	--	-----

## LIST OF FIGURES

	<b>Page</b>
Figure 2.1	Visual representation of the PES for two bimetallic homotops (Borbón, 2011), both clusters have identical shape and number of atoms, but their chemical ordering is different. .... 14
Figure 3.1	A schematic sketch to illustrate the effect of BH transformation on the PES of a one-dimensional example (Wales & Doye, 1997). .....44
Figure 3.2.	Flow chart of the first-stage procedure of two-stage global search algorithm. ....54
Figure 3.3.	Flow chart of the second-stage procedure of two-stage global search algorithm. ....55
Figure 3.4	Cyclic ring cluster $C_{18}$ via "pg9" simulation from the theoretical/computational aspects possess the same structure with the experimental work (Castelvecchi, 2019). .....63
Figure 4.1	Ground states structures of $Al_xTi_yNi_z$ ( $x + y + z = 4$ ) cluster as a function of the atomic composition. Blue sphere represents Ti atoms, red for Al and green for Ni. Number below each model of cluster geometry indicates the number of Al, Ti and Ni atoms in each cluster. ....72
Figure 4.2	LHS is the GS structure given by Erkoc while the RHS is that after the LHS is optimized with B3LYP/6-311G*. (a) The symmetry of the RHS structure agrees with the $Al_2TiNi$ cluster as reported in our present work in Figure 4.1, with a common total energy ( $ET = -77348.708994$ eV). (b) The symmetry of the RHS structure agrees with the $AlTi_2Ni$ cluster as reported in our present work in Figure 4.1. However, the total energy of the RHS is higher by 0.5663 eV when compared to the energy value ( $ET = -93864.435886$ eV). of $AlTi_2Ni$ in Figure 4.1. (c) The symmetry of the RHS structure does not agree with the $AlTiNi_2$ cluster as reported in our present work in Figure 4.1. The total energy of the

	RHS is also higher by 1.1050 eV when compared to the common total energy of $\text{AlTiNi}_2$ ( $ET = -111792.906815$ eV) in Figure 4.1.....	73
Figure 4.3	Average interatomic distance (in Å) of $\text{Al}_x\text{Ti}_y\text{Ni}_z$ ( $x + y + z = 4$ ) clusters as a function of the atomic composition. ....	74
Figure 4.4	Ground states structures of $\text{Al}_x\text{Ti}_y\text{Ni}_z$ ( $x + y + z = 5$ ) cluster as a function of the atomic composition. Blue sphere represents Ti atoms, red for Al and green for Ni. Number below each model of cluster geometry indicates the number of Al, Ti and Ni atoms in each cluster.....	76
Figure 4.5	Average interatomic distance (in Å) of $\text{Al}_x\text{Ti}_y\text{Ni}_z$ ( $x + y + z = 5$ ) clusters as a function of the atomic composition. ....	78
Figure 4.6	Ground states structures of $\text{Al}_x\text{Ti}_y\text{Ni}_z$ ( $x + y + z = 6$ ) cluster as a function of the atomic composition. Blue sphere represents Ti atoms, red for Al and green for Ni. Number below each model of cluster geometry indicates the number of Al, Ti and Ni atoms in each cluster.....	81
Figure 4.7	Average interatomic distance (in Å) of $\text{Al}_x\text{Ti}_y\text{Ni}_z$ ( $x + y + z = 6$ ) clusters as a function of the atomic composition .....	82
Figure 4.8	Binding energy per atom (in eV) of $\text{Al}_x\text{Ti}_y\text{Ni}_z$ ( $x + y + z = 4$ ) clusters as a function of the atomic composition. ....	84
Figure 4.9	Excess energy (in eV) of $\text{Al}_x\text{Ti}_y\text{Ni}_z$ ( $x + y + z = 4$ ) clusters as a function of the atomic composition.....	85
Figure 4.10	Second-order difference energy (in eV) of $\text{Al}_x\text{Ti}_y\text{Ni}_z$ ( $x + y + z = 4$ ) clusters as a function of the atomic composition.....	86
Figure 4.11	Binding energy per atom (in eV) of $\text{Al}_x\text{Ti}_y\text{Ni}_z$ ( $x + y + z = 5$ ) clusters as a function of the atomic composition. ....	87
Figure 4.12	Excess energy (in eV) of $\text{Al}_x\text{Ti}_y\text{Ni}_z$ ( $x + y + z = 5$ ) clusters as a function of the atomic composition.....	88

Figure 4.13	Second-order difference energy (in eV) of $\text{Al}_x\text{Ti}_y\text{Ni}_z$ ( $x + y + z = 5$ ) clusters as a function of the atomic composition.....	89
Figure 4.14	Binding energy per atom (in eV) of $\text{Al}_x\text{Ti}_y\text{Ni}_z$ ( $x + y + z = 6$ ) clusters as a function of the atomic composition. ....	90
Figure 4.15	Excess energy (in eV) of $\text{Al}_x\text{Ti}_y\text{Ni}_z$ ( $x + y + z = 6$ ) clusters as a function of the atomic composition.....	92
Figure 4.16	Second-order difference energy (in eV) of $\text{Al}_x\text{Ti}_y\text{Ni}_z$ ( $x + y + z = 6$ ) clusters as a function of the atomic composition.....	92
Figure 5.1	Chemical order parameter ( $\sigma$ ) of $\text{Al}_x\text{Ti}_y\text{Ni}_z$ ( $x + y + z = 4$ ) clusters as a function of the atomic composition .....	97
Figure 5.2	Chemical order parameter ( $\sigma$ ) of $\text{Al}_x\text{Ti}_y\text{Ni}_z$ ( $x + y + z = 5$ ) clusters as a function of the atomic composition. ....	98
Figure 5.3	Chemical order parameter ( $\sigma$ ) of $\text{Al}_x\text{Ti}_y\text{Ni}_z$ ( $x + y + z = 6$ ) clusters as a function of the atomic composition. ....	99
Figure 5.4	Ionisation potential (IP) (in eV) of $\text{Al}_x\text{Ti}_y\text{Ni}_z$ ( $x + y + z = 4$ ) clusters as a function of the atomic composition. ....	101
Figure 5.5	Electron affinity (EA) (in eV) of $\text{Al}_x\text{Ti}_y\text{Ni}_z$ ( $x + y + z = 4$ ) clusters as a function of the atomic composition. ....	102
Figure 5.6	Global hardness ( $\eta$ ) (in eV) of $\text{Al}_x\text{Ti}_y\text{Ni}_z$ ( $x + y + z = 4$ ) clusters as a function of the atomic composition. ....	103
Figure 5.7	Mulliken electronegativity ( $\xi$ ) (in eV) of $\text{Al}_x\text{Ti}_y\text{Ni}_z$ ( $x + y + z = 4$ ) clusters as a function of the atomic composition.....	103
Figure 5.8	HOMO-LUMO energy gaps (in eV) of $\text{Al}_x\text{Ti}_y\text{Ni}_z$ ( $x + y + z = 4$ ) clusters as a function of the atomic composition.....	104
Figure 5.9	Ionisation potential (IP) of $\text{Al}_x\text{Ti}_y\text{Ni}_z$ ( $x + y + z = 5$ ) clusters as a function of the atomic composition. ....	106
Figure 5.10	Electron affinity (EA) of $\text{Al}_x\text{Ti}_y\text{Ni}_z$ ( $x + y + z = 5$ ) clusters as a function of the atomic composition.....	106

Figure 5.11	Global hardness ( $\eta$ ) of $\text{Al}_x\text{Ti}_y\text{Ni}_z$ ( $x + y + z = 5$ ) clusters as a function of the atomic composition.....	107
Figure 5.12	Mulliken electronegativity ( $\xi$ ) of $\text{Al}_x\text{Ti}_y\text{Ni}_z$ ( $x + y + z = 5$ ) clusters as a function of the atomic composition. ....	108
Figure 5.13	HOMO-LUMO energy gaps of $\text{Al}_x\text{Ti}_y\text{Ni}_z$ ( $x + y + z = 5$ ) clusters as a function of the atomic composition. ....	108
Figure 5.14	Ionisation potential (IP) of $\text{Al}_x\text{Ti}_y\text{Ni}_z$ ( $x + y + z = 6$ ) clusters as a function of the atomic composition.....	111
Figure 5.15	Electron affinity (EA) of $\text{Al}_x\text{Ti}_y\text{Ni}_z$ ( $x + y + z = 6$ ) clusters as a function of the atomic composition.....	111
Figure 5.16	Global hardness ( $\eta$ ) of $\text{Al}_x\text{Ti}_y\text{Ni}_z$ ( $x + y + z = 6$ ) clusters as a function of the atomic composition.....	112
Figure 5.17	Mulliken electronegativity ( $\xi$ ) of $\text{Al}_x\text{Ti}_y\text{Ni}_z$ ( $x + y + z = 6$ ) clusters as a function of the atomic composition. ....	112
Figure 5.18	HOMO-LUMO energy gaps of $\text{Al}_x\text{Ti}_y\text{Ni}_z$ ( $x + y + z = 6$ ) clusters as a function of the atomic composition. ....	113
Figure 5.19	HOMO-LUMO energy gaps with multiplicity $M'$ of $\text{Al}_x\text{Ti}_y\text{Ni}_z$ ( $x + y + z = 6$ ) clusters as a function of the atomic composition.....	117

## LIST OF SYMBOLS

$Al_x$	$x$ -number of Aluminum atoms in Al-Ti-Ni cluster
$Al_xTi_yNi_z$	Al-Ti-Ni cluster with $x$ -number of Aluminum, $y$ -number of Titanium and $z$ -number of Nickel
$E$	Energy
$EA$	Electron affinity
$E_{Al_kTi_lNi_m^-}$	Energy of Al-Ti-Ni anionic cluster
$E_{Al_xTi_yNi_z}$	Energy of Al-Ti-Ni cluster
$E_{Al_xTi_yNi_z^+}$	Energy of Al-Ti-Ni cationic cluster
$E_{exc}$	Excess energy
$E_{gap}$	HOMO-LUMO energy gap
$E_T$	Total energy
$E_b$	Binding energy
$IP$	Ionization potential
$M$	Multiplicity
$M'$	Actual multiplicity
$N$	Total number of atoms/cluster size
$Ni_z$	$z$ -number of Nickel atoms in Al-Ti-Ni cluster
$Ti_y$	$y$ -number of Titanium atoms in Al-Ti-Ni cluster
$n_{Al-Al}$	Number of nearest Al-Al bonds
$n_{Al-Ni}$	Number of nearest Al-Ni bonds
$n_{Al-Ti}$	Number of nearest Al-Ti bonds
$n_{Ni-Ni}$	Number of nearest Ni-Ni bonds
$n_{Ti-Ni}$	Number of nearest Ti-Ni bonds
$n_{Ti-Ti}$	Number of nearest Ti-Ti bonds
$n_{xyz}$	total number of the nearest neighbor

$1/n_{xyz}$	normalization factor
$d$	Interatomic distances between atoms
$\alpha$	$\alpha$ -orbitals
$\beta$	$\beta$ -orbitals
$\eta$	Global hardness
$\xi$	Mulliken electronegativity
$\sigma$	Chemical Order
$\Delta_E$	Second-Order difference energy



## LIST OF ABBREVIATIONS

ADF	Amsterdam Density Functional
Al	Aluminum
Al-Ti-Ni	Aluminum-Titanium-Nickel
AMRD	Angular Movement and Random Displacement
Au	Aurum
B3LYP	Becke three-parameter Lee-Yang-Parr
BH	Basin Hopping
BLYP	Becke Lee-Yang-Parr
CCSD	Coupled Cluster with Single and Double excitations
CCSD (T)	Coupled Cluster with Single and Double excitations plus a perturbative correction for connected Triples
CS	Cut and Splice
DFT	Density Functional Theory
DFTB	Density Functional Tight Binding
Fe	Iron
Fe-Co-Ni	Iron-Cobalt-Nickel
Fe-Co-Pd	Iron-Cobalt-Palladium
G09	Gaussian 09
GA	Genetic Algorithm
GEGA	Gradient Embedded Genetic Algorithm
GGA	Generalized Gradient Approximation
HF	Hartree Fock
HOMO	Highest Occupied Molecular Orbital
IPS	Institut Pengajian Siswazah
KS	Kohn-Sahm
LAMMPS	Large-scale Atomic/Molecular Massively Parallel Simulator
LSDA	Local Spin Density Approximation
LUMO	Lowest Occupied Molecular Orbital
MD	Molecular Dynamics
MP2	Second-Order Møller–Plesset Perturbation Theory
Ni	Nickel
PBE	Perdew-Burke-Ernzerhof

Pd	Palladium
PES	Potential Energy Surface
Pt	Platinum
PTMBHGA	Parallel Tempering Multicanonical Basin Hopping Genetic Algorithm
pg9	PTMBHGA + G09
RKS	Restricted Kohn-Sham
SK	Slater-Koster
SWVN	Slater exchange plus Vosko, Wilk, Nusair
TEM	Transmission Electron Microscope
Ti	Titanium
UKS	Unrestricted Kohn-Sham
XC	Exchange Correlation
ZPE	Zero Point Energy

## LIST OF APPENDICES

- APPENDIX A Multiplicity calculation of all clusters in six atoms aluminium-titanium-nickel clusters system
- APPENDIX B Ni<sub>4</sub>, Ni<sub>5</sub> and Ni<sub>6</sub> ground state structure search with a molecular dynamics approach
- APPENDIX C Comparison of 6-311G\* and LANL2DZ basis sets in the second of the two-stage scheme

**KAJIAN PRINSIP PERTAMA TENTANG SIFAT-SIFAT STRUKTUR,  
KESTABILAN DAN ELEKTRONIK UNTUK KELOMPOK KECIL  
ALUMINIUM-TITANIUM-NIKEL**

**ABSTRAK**

Kelompok nano telah menjadi sistem yang menarik perhatian pada dekad yang lepas disebabkan oleh sifat-sifatnya yang bergantung kepada saiz yang agak luar biasa berbanding dengan struktur susunan pukal, contoh: sifat kimia dan elektronik antara buckminsterfullerene C<sub>60</sub> dan graphene. Walau bagaimanapun, kajian komputasi, teori dan eksperimen untuk kelompok yang bersaiz kecil untuk unsur tulen dan perduaan adalah terhad, apatah lagi kelompok yang bersaiz nano bagi unsur ternari. Untuk kes kelompok aluminium-titanium-nikel (Al-Ti-Ni), kebanyakannya karya terbitan tentang kelompok-kelompok kecil Al-Ti-Ni berasal dari Erkoc dan Oymak (2003; 2002, 2004) dengan menggunakan potensi empirik yang asas dalam teknik dinamik molekul, diikuti dengan melakukan pengoptimuman titik tunggal pada tahap DFT untuk mendapatkan struktur keadaan asas untuk kelompok tersebut. Penerbitan kelompok Al-Ti-Ni (Aluminum-Titanium-Nikel) yang bersaiz kecil kebanyakan adalah dihasilkan oleh Erkoc and Oymak. Kelompok Al-Ti-Ni secara umumnya mempunyai ciri-ciri mekanikal dan pemangkinan yang sangat berbeza berbanding dengan struktur susunan pukal seperti yang dinyatakan dalam karya terbitan oleh Erkoc dan Oymak (2003; 2002, 2004). Namun demikian, maklumat dan data mengenai sifat pemangkin dan mekanikal kelompok-kelompok Al-Ti-Ni tidak ditunjukkan dalam artikel mereka. Dalam karya terbitan mereka, kekurangan sokongan data darip eksperimen bagi sebahagian besar struktur keadaan asas dari kelompok-kelompok unsur perduaan and ternari kelompok Al-Ti-Ni merupakan salah satu sebab untuk kes ini berlaku. Tesis ini

melaporkan kajian yang bersistematis mengenai pemodelan komputasi untuk kelompok-kelompok Al-Ti-Ni yang bersaiz kecil pada peringkat atomistik dengan menggunakan strategi pengiraan berperingkat dua secara bertaktik dan juga pelbagai alat teoritis. Fokus utama tesis ini adalah untuk melakukan kajian yang bersistematis dan teliti terhadap ciri-ciri yang terpilih daripada kelompok  $Al_xTi_yNi_z$  pada keadaan tenaga terendah, yang mana  $x$ ,  $y$  dan  $z$  adalah integer positif, dengan  $x + y + z = 4, 5$  and  $6$ . Konfigurasi tenaga keadaan asas kelompok diperoleh dengan melakukan pengoptimuman berperingkat dua yang direka khas. Pada peringkat pertama, algoritma "pg9" (juga dikenali sebagai Parallel Tempering Multicanonical Basin Hopping and Genetic Algorithm (PTMBHGA) yang digabungkan dengan kalkulator teori fungsi ketumpatan (DFT) (Gaussian 09, disingkat G09)) untuk mengkaji struktur "low-lying" (LLS) secara statistik dengan menggunakan fungsi korelasi pertukaran -SVWN dan calon set asas yang lebih sesuai. STO-3G, 3-21G dan 6-31G adalah tiga set asas yang berbeza dengan kerumitan komputasi rendah yang digunakan untuk melakukan simulasi percubaan kepada beberapa sampel kelompok yang dipilih dari sistem kelompok Al-Ti-Ni. Sebagai hasilnya, SVWN / 3-21G adalah fungsi korelasi pertukaran dan set asas yang sesuai untuk mengkaji LLS kelompok Al-Ti-Ni secara statistik dalam tesis ini berdasarkan jumlah fungsi asas dan kos pengiraannya tersebut. Pertama, konfigurasi kluster awal yang rawak dioptimumkan secara global dengan menggunakan algoritma BHGA (basin hopping and genetic algorithm), iaitu satu cara carian tidak berat sebelah dalam algoritma "pg9" dengan menggunakan fungsi korelasi pertukaran dan set asas dengan kerumitan pengiraan yang rendah. Pada peringkat kedua, konfigurasi tenaga terendah yang diperolehi daripada peringkat pertama dioptimumkan lagi dengan menggunakan algoritma carian BHGA dalam algoritma "pg9", tetapi pada kali ini fungsi korelasi pertukaran dan set

asas yang lebih bermutu digunakan. Kaedah yang berperingkat dua ini dapat menghasilkan struktur keadaan asas yang boleh dipercayai bagi kelompok  $Al_xTi_yNi_z$  yang kecil pada peringkat DFT. Fungsi korelasi pertukaran dengan dua set asas yang lebih bermutu, iaitu B3LYP / LANL2DZ dan B3LYP / 6-311G \* digunakan untuk melakukan simulasi percubaan pada beberapa sampel kelompok untuk simulasi peringkat kedua. Akhirnya, B3LYP / 6-311G \* dipilih sebagai fungsi korelasi pertukaran dan set asas yang lebih yang untuk simulasi peringkat kedua kerana fungsi korelasi pertukaran dan set asas ini dapat menghasilkan kelompok dengan lebih simetri dan nilai jumlah tenaga dengan lebih rendah berbanding dengan B3LYP / LANL2DZ. Selepas konfigurasi keadaan asas kelompok-kelompok Al-Ti-Ni yang dioptimumkan diperolehi, tenaga dan geometri mereka akan diselidiki dan dibandingkan. Di samping itu, struktur elektronik kumpulan Al-Ti-Ni juga dikaji dengan melakukan satu siri perhitungan untuk susunan kimia, potensi ionisasi, afiniti elektron, kekerasan global dan sebagainya. Dalam tesis ini, teknik dinamika molekul juga dilakukan pada kelompok tertentu sistem kluster Al-Ti-Ni ini dengan menggunakan algoritma "plmp" (juga dikenali sebagai PTMBHGA yang digabungkan dengan Atomic Molecular Massively Parallel Simulator (LAMMPS) sebagai kalkulator tenaga) dan ditunjukkan dalam lampiran. Seterusnya, jumlah nilai tenaga kelompok-kelompok Al-Ti-Ni diperolehi dengan melakukan pengoptimuman pada tahap DFT dengan menggunakan "pg9". Nilai tenaga keseluruhan struktur kelompok yang dihasilkan dengan menggunakan kaedah "plmp + pg9" dua peringkat lebih tinggi jika dibandingkan dengan kelompok yang sama yang menjalani prosedur dua peringkat pada tahap DFT yang dinyatakan dalam tesis ini. Secara umumnya, sebahagian besar struktur keadaan asas kelompok unsur tulen dan perduaan yang dihasilkan dalam tesis ini serupa dari segi geometri dengan literatur yang ada dari penyelidik lain. Secara keseluruhannya,

hasil struktur keadaan asas kelompok-kelompok unsur tulen dan perduaan dalam tesis ini adalah sepadan dengan penerbitan yang sedia ada. Keputusan baru yang diperolehi dalam tesis ini termasuk (i) struktur keadaan asas unsur terneri  $\text{Al}_x\text{Ti}_y\text{Ni}_z$  ( $x + y + z = 4, 5 \text{ \& } 6$ ) yang jarang atau tidak dilaporkan dalam literatur, (ii) kluster yang kaya dengan Ni menunjukkan nilai tenaga pengikatan dan tenaga berlebihan yang terendah, dan nilai tenaga perbezaan kedua dan jurang tenaga HOMO-LUMO yang tertinggi.

# **FIRST-PRINCIPLES STUDY OF STRUCTURAL, STABILITY AND ELECTRONIC PROPERTIES OF SMALL ALUMINUM-TITANIUM- NICKEL CLUSTERS**

## **ABSTRACT**

Nanocluster has been a system of interest for the past decades due to its peculiar size-dependent properties as compared to its bulk counterparts, e.g. the chemical and electronic properties between the buckminsterfullerene C<sub>60</sub> and graphene. However, computational, theoretical and experimental studies for pure and binary element small-size clusters are scarce, not to mention of small-size ternary element clusters. For the case of aluminium-titanium-nickel (Al-Ti-Ni) ternary element clusters, published works of small Al-Ti-Ni clusters mostly come from Erkoc and Oymak (2003; 2002, 2004) by using a fundamental empirical potential in molecular dynamic techniques, followed by performing a single point optimization at DFT level to obtain the ground-state structure for the cluster. The Al-Ti-Ni clusters generically have a very different mechanical and catalytic properties compared to their bulk counterparts, as stated in the articles by Erkoc and Oymak (2003; 2002, 2004). However, information and data about the catalytic and mechanical properties Al-Ti-Ni clusters are not shown in their articles. One of the reasons for this to have happened is that most of the ground-state structure of the binary of ternary element Al-Ti-Ni clusters that shown in their article are lack of experimental data supports. This thesis reports a systematic study of the computational modelling of small-size Al-Ti-Ni clusters at the atomistic level using a tactical two-stage computational strategy and a multitude of theoretical tools. The main focus of this thesis is to perform a systematic and thorough study on selected properties of the Al<sub>x</sub>Ti<sub>y</sub>Ni<sub>z</sub> clusters at the lowest energy state, where  $x$ ,  $y$  and  $z$  are non-negative



integers such that  $x + y + z = 4, 5$  and  $6$ . The ground state energy configurations of the clusters are obtained by performing a purpose-designed two-stage optimization. In the first stage, the "pg9" algorithm (a.k.a Parallel Tempering Multicanonical Basin Hopping and Genetic Algorithm (PTMBHGA) that is coupled to a density-functional theory (DFT) calculator (Gaussian 09, abbreviated G09)) to study the low-lying structures (LLS) of the cluster statistically by exchange-correlation functional -SVWN with a suitable basis-set candidate. Three different basis sets (STO-3G, 3-21G and 6-31G) with low computational complexity are employed to perform trial simulations to several cluster samples that were chosen from Al-Ti-Ni clusters system. As a result, the SVWN/3-21G is the suitable exchange functional and basis set to study the LLS statistically of the Al-Ti-Ni clusters in this thesis based on its number of basis functions and computational costs. First, the configuration of a randomly initialised cluster is globally optimized using an unbiased search algorithm BHGA (Basin Hopping and Genetic Algorithm) in "pg9" algorithm that uses an exchange-correlation functional and basis sets with low computational complexity. In the second stage, the lowest-energy configuration obtained from the first stage is further optimized using the BHGA algorithm, but a higher quality of exchange-correlation functional and basis set are employed at the second-stage simulation instead. A better quality exchange-correlation functional with two basis sets – B3LYP/LANL2DZ and B3LYP/6-311G\* are employed to perform trial simulations on several cluster samples for the second-stage simulations. At last, B3LYP/6-311G\* is chosen as a suitable exchange-correlation functional and basis set in second-stage simulations because this set of exchange-correlation functional and basis set able to produce the cluster with more symmetry and total energy with lower value compared to the B3LYP/LANL2DZ. The two-stage procedure can produce reliable ground state structures of small  $Al_xTi_yNi_z$

clusters at the DFT level. After the ground state configurations of the optimized clusters are obtained, their energetic and geometrical are investigated and compared. In addition, the electronic structures of the Al-Ti-Ni clusters are also studied by performing a series of calculations for their chemical order, ionization potential, electron affinity, global hardness, etc. In the appendix of this thesis, molecular dynamics technique also performed on certain clusters of this Al-Ti-Ni clusters system by using "plmp" algorithm (a.k.a PTMBHGA integrated with Large-scale Atomic/Molecular Massively Parallel Simulator (LAMMPS) as energy calculator). Next, the total energy value of these clusters is obtained by performed an optimization on them at DFT level by using "pg9". The total energy value of these cluster structures that generated by employing a two-stage "plmp+pg9" method is higher than the same clusters that undergo the two-stage procedure at DFT level that stated in this work. In general, most of the ground state structure of pure and binary element clusters produced in this thesis are similar in term of geometry with the available literature from other researchers. The new results obtained in this thesis include (i) the ground state structure of ternary element  $Al_xTi_yNi_z$  ( $x + y + z = 4, 5 \& 6$ ) that are rarely or never be reported in the literature, (ii) Ni-rich clusters show minimum value in the binding energy and excessive energy, and maximum value in the second difference energy and HOMO-LUMO energy gap.

# CHAPTER 1

## INTRODUCTION

Nature isn't classical, dammit, and if you want to make a simulation of nature, you'd better make it quantum mechanical, and by golly, it's a wonderful problem because it doesn't look so easy. –R. P. Feynman (1982) –

The concept of miniaturization was introduced a few decades ago; however, its development does not arrive at the saturation stage. In fact, engineers and researchers still attempt to shrink the size of the electronic, optical and mechanical devices in order to make these devices become smaller. Wide range of extraordinary and advanced technological applications, from industrial (such as catalytic process, magnetic storage, etc.) to medical (as in cancer diagnosis) application is the greatest motivation to study and develop nanotechnology.

Today, size of the nanoparticles (e.g. nanoclusters) with diameters much less than 50 nm are capable of being fabricated, manipulated and even visualized at the atomic scale or even quantum scale by experimentalist with the assistant of the state-of-the-art experiment instruments. At the same time, high-performance computational technologies have been advancing rapidly since last decades, and theorists managed to proposed new insight, idea and algorithms (such as intelligent search or A.I.) to perform vigorous investigation properties and applications of nanoparticles, as well as design a new material by carrying out in silico experiments with the high-performance computational resources. In this chapter, motivations and the problems statement to study the Al-Ti-Ni nanocluster are stated, this followed by objectives and background studies of this cluster system. In the end, the thesis outline s presented on this work.

## 1.1 Motivation

Due to advancement in nanotechnology, interest to explore new generation of nanomaterials with exotic functionalities are surging. Nanoclusters, one of those advanced materials, comprised of a finite number of atoms closely bonded to each other by atomic forces. The number of atoms that makes up a cluster,  $N$ , is normally referred as the size of the nanocluster, which behaves very differently when compared to a single atom, molecule or bulk solid. Strictly speaking, the structural and energetic behaviour of the changes, in all probability, as the cluster is varying with size  $N$  (Taherkhani & Rezania, 2012).

The main aims of this study include understanding, predicting the structural and electronic properties of Al-Ti-Ni nanocluster systems. The Al-Ti-Ni ternary system is an important subsystem of nickel-based alloys and has been widely used in the aerospace industry, as these materials have outstanding mechanical properties and corrosion resistance at high temperatures (Duan et al., 2019). Increasing the content of titanium in the Al-Ti-Ni system will harder the product (Riyadi, 2020). The understanding of the properties of the Al-Ti-Ni system is essential in order to fully utilize this alloy in heat resistant material manufacturing. In particular, the structural, electronic and thermal properties of Al-Ti-Ni nanoclusters have not been well studied so far. Studying the properties of Al-Ti-Ni ternary alloy at the nanoscale through experiments is ultimately challenging, yet no experimental investigation on a small scale Al-Ti-Ni nanoclusters (less than the size of 20 nm diameter) has been published so far. Theoretical modelling and computational simulation hence provide a convenient and viable approach to complement experimental investigation of nanoscale Al-Ti-Ni nanoclusters.

Experiments on a free-standing pure element atomic clusters are rarely reported, so are small, multi-element atomic clusters. To bridge the gap caused by the rarity of experimental data, the understanding of physical properties of single element and multi-element

nanoclusters calls for complementary insight through reliable theoretical modelling. Many modern functional materials, such as barium titanate ( $\text{BaTiO}_3$ ), yttrium barium copper oxide (YBCO), buckminsterfullerene ( $\text{C}_{60}$ ), graphene or other 2D materials are well supported by reliable results from theoretical and experimental efforts. As such, establishing the ground state structures of these popular materials is a relatively straight-forward effort. However, this is not so for specific multi-element nanoclusters such as the subject of study in this thesis. The ground state structure, which is the very essential prerequisite information required has to be ascertained before further knowledge about the physical properties of these nanoclusters can be abstracted.

There are many occasions in which the detailed atomistic structure of a bulk or nanomaterial are not known due to either the lack of empirically measured data or relevant theoretical information. To make up for the absence of the crystal structure information, educated guess can be made by using cluster seed method, viable theoretical consideration, pure mathematical algorithm, or adaption of an assumed structure. These are loosely referred to as 'biased' methods. A specific example of 'biased method' is that exemplified in the paper by Ramírez (2011). The author used General Embedded Genetic Algorithm (GEGA, which is an unbiased method) to generate the structural geometry of single element nanoclusters. Without repeating the unbiased search, the author assumed the geometries of other multi-element nanoclusters are the same as that of the single element nanoclusters. In this case, the generalisation is done without providing strong experimental and theoretical justification, hence 'biased'. A biased method is a computationally easy and convenient way to mock the geometrical information needed as the input in a DFT or MD calculation. However, the 'biased' structures so obtained are, for obvious reason, not as reliable due to excessive pre-assumptions in the algorithm used to generate them. A wrong input structure will result in large discrepancy in the physical properties predicted by DFT especially for the case of multi-element nanoclusters. In this study, instead of unbiased, an unbiased

search algorithm will be adopted to obtain the ground-state structure of aluminium-titanium-nickel nanoclusters. In an unbiased search process, the initial structures are first generated randomly. They are then progressively modified and optimized by the intelligent optimization algorithm (such as basin hopping, genetic algorithm or even neural network) in subsequent rounds of iteration until a supposedly 'global' minima is arrived. The optimized structure with a globally minimized energy (which is taken as the ground state structure) is then further investigated using DFT. This procedure is done without making any biased assumptions from the beginning, hence the term 'unbiased'.

## **1.2 Problem statement**

The theoretical works reported on the unusual size-dependent properties of trimetallic nanoclusters are scant compared to those structural, electronic, catalytic and magnetism properties reported in pure and bimetallic clusters. Due to the order-of-magnitude cheaper computational cost, many computational modelling works on large clusters are conducted using the molecular dynamics (MD) method, which speed is accelerated with the employment of empirical potentials. The reliability of the results from MD greatly depends on the quality or suitability of the potential employed. Here, a cluster is defined 'large' when the number of atoms exceeds ~30. This is a small number for MD but a relatively large figure from the practicality viewpoint of first-principles calculations. The number of theoretical published work using unbiased search with density functional theory (DFT) method to study the structural and electronic properties on ternary clusters is relatively rare, partly due to the expensive computational cost, as well as the technical complication to implement an effective global search algorithm involving DFT calculators.

There are two types of formalisms commonly used in DFT calculations of clusters, namely, plane-wave basis and linear combinations of atomic orbitals (LCAO) approach. It is generally agreed that the former is more suitable for periodic systems; meanwhile, the latter is for finite systems. In the literature about Al-Ti-Ni clusters, LCAO is the only formalisms applied for the calculations of Al-Ti-Ni clusters at the DFT level. It turns out that some unsettled inconsistency in the results of published works on small  $Al_xTi_yNi_z$  ternary clusters is yet to be resolved, mainly due to the lack of reliable theoretical and experimental evidence on the geometrical structures of these clusters. To the best of our knowledge, the number of published works on the lowest-energy structures of Al-Ti-Ni clusters is extremely scarce, and most of them came from Erkoc et al. (2003; 2002, 2004). In fact, the Al-Ti-Ni structures with the lowest energy reported by Erkoc et al. (2003; 2002, 2004) were obtained by performing search algorithms that coupled to empirical potentials calculator instead of that based on first-principles such as DFT. As such, the ground state structures of small Al-Ti-Ni clusters at the DFT level, which is sitting at a higher level in the hierarchy of theoretical reliability as compared to empirical approaches, are still lacking.

### **1.3 Objectives of study**

This thesis is aspired to provide a detailed density functional theory (DFT) computational study on the ternary Al-Ti-Ni clusters with a different composition and size (with a total atom number  $N$  equal 4 to 6). The objectives of this study include:

1. Determine the lowest-energy configurations of the Al-Ti-Ni system up to a maximum of 6 atoms. The search for the global minimum of a specific cluster is implemented via a two-stage optimization procedure:
  - The first stage - perform an unbiased search for the lowest-energy structure of a cluster in the potential energy surface (PES) generated by an exchange-correlation and basis set with lowest computational complexity as implemented in a chosen DFT calculator.
  - Second stage - a low-lying structure that obtained from the first stage is undergoing vigorous optimization by using a higher quality exchange-correlation and basis-set in the DFT calculator.
2. Further examined the accuracy and authenticity of this vigorous two-stage optimization procedure by using various type of XC/basis-sets in DFT calculator during the scanning potential energy surface and searching ground structure for the small ternary Al-Ti-Ni clusters.
3. Perform a first-principles study and investigations on these small ternary clusters to acquire thorough physically-pertinent information of the electronic structures of the clusters, including their binding energy, excess energy, second-order difference, chemical order, ionization potential, electron affinity, global hardness, Mulliken electronegativities and HOMO-LUMO gaps over the clusters.

#### **1.4 Background studies of Al-Ti-Ni nanoclusters**

Atomic clusters are aggregates of atoms ranging from a few to thousands of atoms or molecules. Nanoclusters are atomic clusters with a diameter in the order of nanometers. They exhibit distinctly different electronic and structural behaviours compared with their larger size counterpart due to low dimensional and quantum confinement effects (Ramírez et al., 2011). From the year 2000 onward, transition metal clusters had been intensively studied, both experimentally (Baletto & Ferrando, 2005;



Parks et al., 1994; Parks et al., 1995; Martin, 1996; Parks et al., 1998; Parks et al., 2000) and computationally (Aprà et al., 2006; Arias et al., 2007; Calaminici et al., 1996; Chang & Chou, 2004; Chou et al., 2009; Chou et al., 2013; Datta et al., 2017; Doye & Wales, 1998; Elliott et al., 2009; Grigoryan & Springborg, 2003; Gupta, 1981; Hu et al., 2009; Lathiotakis et al., 1995; Li & Scheraga, 1990; Longo & Gallego, 2006; –L. Wang & Johnson, 2007; Massobrio et al., 1995; Montejano-Carrizales et al., 1996; Oviedo & Palmer, 2002; Piotrowski et al., 2010; Wales & Doye, 1997; Yang et al., 2006). Nanoclusters, mainly binaries or ternaries, have attracted much attention due to their broad applications in catalysis (Henry, 1998; Joo et al., 2001; Valden et al., 1998), magnetic-recording materials (Entel et al., 2008), and biological applications (e.g., carbon cluster act as an inert capsule to deliver medicine to the human body), to name a few. For example, FeAlAu<sub>n</sub> ( $n = 1 - 6$ ) (J. –F. Zhang et al., 2015), Fe-Co-Ni (Ramírez et al., 2011; Ramírez et al., 2013; Varas et al., 2015), Fe-Co-Pd, (Varas et al., 2016) and AgAuPd (S. Zhao et al., 2017) trimetallic clusters have been studied for their magnetic, electronic, and structural properties.

To investigate the physical and chemical properties of a nanocluster requires the understanding of the conditions under which one structure is more probable than another. The search for the most probable structure, known as the ground state structure, involves a strong interplay of experiment with theory and numerical simulation. By definition, a ground state structure is the state with the lowest minimal energy or known as the global minimum in the PES. The search for GS of a nanocluster is by no means a trivial task as there are practically infinite possible ways a cluster comprised of  $n$  types of an atom could organize themselves. Given the interactions among the atoms are known (which in practice is provided by a total energy calculating program or energy calculator), the search for a structural configuration of the atoms in 3-D space that

minimizes the total energy is a highly non-trivial task. In practice, one could use experimental data as the initial input. Lowest energy structures are then obtained by optimizing the input structure using a local minima search algorithms such as BFGS or conjugate gradient algorithms which are built-in by default in many atomistic computation codes (such a local minimization is also known as 'relaxation'). Quantum mechanical or molecular dynamics calculations for their physical properties are then performed based on these relaxed structures.

In the search for the ground state structures of ternary alloy clusters, one common practice is to generate them based on classical and semiclassical methods such as the adoption of Gupta potential, Sutton-Chen potential, and others empirical potentials. The resultant ground state structures of the small clusters are normally in the shape of an icosahedron. In contrast, truncated octahedron and truncated decahedral structure are favoured by large clusters (Baletto & Ferrando, 2005). Structural evolution of cluster can be explained and tackled by classical and semiclassical approaches, but these methods may fail if the electronic effects from valence electrons of the atoms are taken into account (Ramírez et al., 2011; Ramírez et al., 2013; Varas et al., 2015). Using classical and semiclassical approaches in search of ground-state configurations of transition metal clusters will produce unreliable results, due to the existence of localized d orbitals (Chen et al., 2010; Hao et al., 2007; Hua et al., 2013; Oymak & Erkoc, 2004).

Electronic structure and stability of transition metal clusters, such as intermediate size 3d/4d element clusters (especially 13-atom cluster), have been studied extensively by using density functional theory (DFT) methods (Aprà et al., 2006; Arias et al., 2007; Chang & Chou, 2004; Chou et al., 2009, 2013; Datta et al., 2017, 2017; Grigoryan & Springborg, 2003; Hu et al., 2009; Longo & Gallego, 2006; –L. Wang &

Johnson, 2007; Massobrio et al., 1995; Oviedo & Palmer, 2002; Piotrowski et al., 2010) in the last two decades. However, the simulation results fluctuate with different DFT software and optimization methods employed (Chen et al., 2010; Erkoc & Oymak, 2003; Hao et al., 2007; Hua et al., 2013). In DFT calculations, structural and energy values for a nanocluster might be different due to various types of exchange-correlation (XC) functional and basis set employed in the calculation, for example, Ag<sub>13</sub> and Cu<sub>13</sub> nanocluster that had been reported by applying either Gaussian orbital or plane-wave-based DFT (Arias et al., 2007; Chou et al., 2009; Granja et al., 2008; Hu et al., 2009; Piotrowski et al., 2010). DFT results also vary with inclusion or non-inclusion of semi core states in the pseudopotential (Entel et al., 2008; Michelini et al., 2004).

Currently, a few theoretical works on small size nanoclusters binary alloy of Al-Ti, Al-Ni, and Ti-Ni can be found. Based on theoretical and experimental studies on Al-Ti, Al-Ni, and Ni-Ti binary alloy systems (Du & Clavaguera, 1996; Hong et al., 1990; Lauer et al., 1999; Rhee et al., 1999; Widom & Moriarty, 1998) and ternary alloy system Al-Ti-Ni (Farkas et al., 1996; Huneau et al., 1999; Zeng et al., 1999), these binary and ternary alloy clusters might have the potential to act as a catalyst in industrial engineering (Oymak & Erkoc, 2004). Research done using DFT includes aluminum-doped titanium clusters AlTi<sub>n</sub> ( $n = 1 - 13$ ) by Xiang et al (2004), titanium-doped aluminum clusters Al<sub>n</sub>Ti ( $n = 2 - 24$ ) by Hua et al (2013), electronic and structural properties of Al-Ni clusters ( $n < 5$ ) by Zhao (2017) and coworkers, and bimetallic Ti-Ni clusters ( $n < 13$ ) by Chen et al (2010). In contrast, the literature on global search and generation of ground-state structures of trimetallic clusters by employing full *Ab initio* method is very scarce. Trimetallic nanoclusters Fe<sub>x</sub>Co<sub>y</sub>Pd<sub>z</sub> ( $x + y + z = 7$ ) (Varas et al., 2016) and Fe<sub>x</sub>Co<sub>y</sub>Ni<sub>z</sub> ( $x + y + z = 5, 6, 7, 13$ ) (Ramírez et al., 2011; Ramírez et al., 2013; Varas et al., 2015) were studied for its interesting electronic and magnetic properties.

The structural and electronic properties of  $\text{Al}_k\text{Ti}_l\text{Ni}_m$  ( $k + l + m = 2, 3, 4$ ) (Erkoc & Oymak, 2003; Oymak & Erkoc, 2002) and  $\text{Al}_n\text{Ti}_n\text{Ni}_n$  ( $n = 1 - 16$ ) (Oymak & Erkoc, 2004) clusters had been investigated by Erkoc and Oymak. Al-Ti-Ni cluster structures are generated by these authors based on a molecular dynamics (MD) scheme that applies Lennard-Jones (for a two-body part) and Axilrod-Teller triple-dipole potentials (for three-body parts) (Axilrod & Teller, 1943), whereas the electronic properties of the obtained structures are evaluated via DFT calculations within the Becke three-parameter Lee-Yang-Parr (B3LYP) and effective core potential level. Complementing the work done by these authors, an unbiased search for the ground states structures of  $\text{Al}_k\text{Ti}_l\text{Ni}_m$  clusters employing full DFT calculations has been carried out in this thesis.

## 1.5 Thesis outline

Up to this point, a brief introduction about the motivation and objectives of this thesis has been given in Sections 1.1 and 1.2. In Section 1.3, a general introduction of atomic clusters and previous works related to Al-Ti-Ni clusters that highlight the gap in the theoretical understanding of Al-Ti-Ni clusters will serve as the motivation of this research.

Chapter 2 discusses the theoretical frameworks that form the basis of the methods employed in this project. It starts from the fundamental understanding of computational modelling techniques, followed by the basic ideas and theoretical basis of DFT.

The methodology (computational details), including the computational protocol employed, parameters and approximations used in this project, is given in Chapter 3. It starts from the fundamental understanding of computational modelling techniques,

followed by the conventional optimization approaches to locate the global minimum in a potential energy surface.

In Chapter 4, geometrical structures of the Al-Ti-Ni clusters obtained by using the robust two-stage full DFT method developed in this thesis are reported in detail. The results are then discussed and compared with that reported in the literature. Following this, the optimized configurations are investigated from the energetic and geometrical aspects in order to study their structural and stability properties.

The electronic structures of the optimized Al-Ti-Ni clusters are explored in Chapter 5. In this chapter, chemical order is investigated in order to understand the mixing and segregating of atoms in the clusters. This is followed by the discussion on the electronic properties of the clusters, which include ionization potential, electron affinity, global hardness, Mulliken electronegativities and HOMO-LUMO gaps over the clusters.

Lastly, the thesis is concluded in Chapter 6. The chapter also gives suggestions on how to improve the present computational modelling technique and other possible directions as extensions of work done in this thesis. This thesis presents two appendices: Appendix A illustrates some of the Al-Ti-Ni six atoms clusters with different multiplicity,  $M$ . Appendix A displays the results of zero-point energies and polarizabilities of Al-Ti-Ni clusters optimized from DFT.

## CHAPTER 2

### LITERATURE REVIEW

This chapter gives an overview of computational techniques on nanoclusters, followed by the literature review on density functional theory (DFT) used in this work is discussed. The last section reviews previous works, both biased and unbiased computational works that are related to nanoclusters.

#### **2.1 Computational simulation techniques on nanoclusters**

Obtaining the configurations of the aluminium-titanium-nickel (Al-Ti-Ni) trimetallic clusters with the lowest potential energy, also known as the ground-state structure, is one of the main major objectives of this thesis. Presently, the size of the clusters that can be synthesized by experimentalists in a laboratory using magnetic sputtering or gas aggregation source is in the range of 1 to 100 nm (Deng et al., 2017; Mainet et al., 2012), which is an aggregation of  $\sim 10^2$  to  $\sim 10^8$  atoms. In the latest research, the size of the PdPt nanocluster that can be grown by using gas aggregation source techniques is in the range of 4 to 5 nm, obtained by TEM analysis (Deng et al., 2017; Mainet et al., 2012). Quite commonly, laboratory synthesis of clusters produces mostly large clusters with a number of atoms exceeding  $\sim 100$ . One can measure and observe the shape and size of these synthesized clusters using various experimental techniques such as electron microscopy.

Theoretically, for clusters with large size or number of atoms, locating their ground state structure is not a trivial task, and to some extent can be quite ambiguous in the sense that the configuration space is simply too large. On the other hand, small clusters, e.g., those with the number of atoms less than ten or those with size less than 1 nm, are relatively difficult to synthesized experimentally. As such, the task of

determining the ground state geometry of a small cluster experimentally is pragmatically very difficult. This is even more so for small clusters composed of multiple atom types, such as the trimetallic clusters, the subject considered in this thesis. In the even the geometrical shape of a small multiple atom type cluster is measured experimentally, the result could be further strengthened if it could be complemented by a conforming theoretical prediction.

From the theoretical point of view, the interactions between atoms in a system can be described by classical or quantum approaches. Different potential energy surfaces (PES) of the system can be calculated by using either empirical potential (classical approaches) or density functional theory (DFT) (quantum mechanical approaches). Wales (2003) shows that the PES of a cluster, as a function of coordinates, can be represented in the form of a diagram. A cluster with  $N$  number of atoms will possess a  $(3N + 1)$ -dimensional PES, where  $3N$  represents the degrees of freedom while the extra one dimension is the potential energy of the system. The PES of two bimetallic cluster homotops as a function of the  $3N$ -dimensional vector of Cartesian coordinates are illustrated in Figure 2.1. Figure 2.1 shows the PES of two bimetallic cluster homotops as a  $3N$ -dimensional of Cartesian coordinates. Both clusters possess an identical number of atoms and geometries. Both of the cluster systems also comprised of two types of elements A (blue) and B (grey).

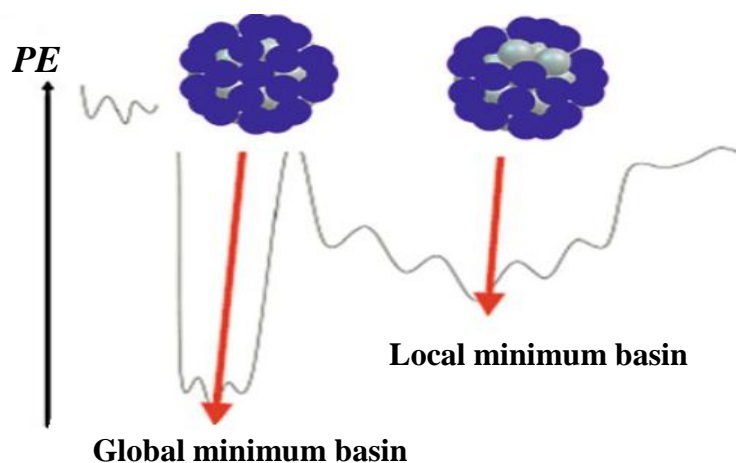


Figure 2.1 Visual representation of the PES for two bimetallic homotops (Borbón, 2011), both clusters have identical shape and number of atoms, but their chemical ordering is different.

However, the energy state of the system changed due to the effect of varying chemical order. As shown in the diagram, the cluster at the left that located the global minimum basin is the configuration that possesses the lowest potential energy in the system. It is also known as ground state structure while the configuration at the right refers to one of the local minima basins of the system, also known as low-lying structure (LLS).

In the literature, the interaction among the atoms in a system is described by a spectrum of approaches. Largely, they can be categorized into two major types, namely the empirical and first-principles approaches. The classical method, such as molecular dynamics (MD) that employs empirical potential is able to explore the PES of a cluster system. Due to its nature of being empirical, hence a cheap computational cost, MD enjoys the benefit of a much-reduced cost in simulation time. In simple molecular system such as that composed of Lennard-Jones (LJ) particles, the interaction between the atoms is described in terms of attractive and repulsive parameters, which are determined by fitting the LJ potential against experimental data. However, the LJ potential can only describe prototypical systems in which the particles are interacting via the simple van der Waals forces, e.g., a rare gas system (Wales & Doye, 1997). For systems containing interaction beyond the LJ potential, such as metallic bonding effect, extra physical contributions beyond the simple LJ-type attractive and repulsive parameters have to be taken into consideration. Many advanced beyond-LJ-type empirical potentials involve three-body interaction terms to cater for experimentally measurable effects not captured by the prototypical LJ potential such as charge transfer and bond breaking. Generally, such these are known as 'many-body potentials'. Examples of many-body potentials are the Gupta potential (1981), embedded-atom-



model (EAM) (Daw & Baskes, 1983) and charged optimized many-body potential (COMB3) potentials (T. Liang et al., 2013). These are widely used by the MD community and are found in common MD packages such as LAMMPS (Plimpton, 1995). Generally, interatomic potentials from MD are fit to a specific application and material. Bulk energetics, defects, and mechanical properties are the most commonly fitted properties, especially for bulk solid-state materials. All these quantities are obtained from experiments when available, or quantum mechanical calculations such as density functional theory (DFT) simulations (Choudhary et al., 2017). It is possible to locate the global minimum of a metallic cluster by using classical approaches such as MD. However, the reliability of the results that are generated by using empirical potential in MD is often questionable as the treatment of the electron-electron interaction are not taken into account. The PES of a cluster system cannot be reliably scanned for a global minimum if the force-field (a.k.a., potential) itself does not correctly capture the correct or essential aspects of the physics of the system in the first place. In other word, the reliability and availability of the force-fields for simulating a cluster system is the bottleneck for securing a reliable prediction of its ground state structures.

Unlike MD, first-principles calculations, e.g., DFT does not require any empirical parameters for calculating the total energy of a cluster. To calculate the total energy of a cluster, in principle, only the identities and spatial locations of the atoms in the system are required as input. The energies associated with the interactions among the atoms due to the contribution from all the electrons in the atoms comprising the cluster are computed quantum mechanically from the first-principles. Due to its nature as being fundamentally quantum mechanical, the first-principle calculation is computational intensive in practice. It is a feasible assumption that the ground state

geometry and total energy of a cluster which are obtained from scanning the PES of the cluster system using first-principles calculations are more reliable than that obtained via MD.

There are two major types of first-principles methods: Hartree-Fock approximation (HF) and density functional theory. In the HF approach, the many-electron wave function of a system is constructed from the products of single-electron wave functions (Slater determinant). In a quantum mechanical system of many-body, exchange-correlation effects that arise due to the non-locality nature of the quantum law, have to be catered for in a computational scheme for solving the Schrodinger equations describing the system. In the prototypical HF approach, the Slater determinant only captures the exchange aspect of the non-locality effect but not the quantum correlated motions of electrons. The neglect of electron correlation, more precisely the Coulomb correlation, in the HF description is at the root of the inadequacy of HF wavefunction in describing the real atoms and molecules. Various enhanced versions of post-HF calculation schemes have been proposed to cater for the shortfall to cater for the quantum correlation effect in prototypical HF calculation schemes. These post-HF schemes demand a proportionally higher computational cost for better quality performance in accuracy and reliability, usually denoted via the hierarchical order: CCSD(T) > CCSD > MP2 > HF. The acronyms refer to various enhanced versions of the post-HF calculation scheme.

In this thesis, the first-principles method deployed is DFT. A more detailed description of this calculation scheme is presented in the following section.

## 2.2 Density functional theory

*Ab initio* is defined as "from the beginning" or "from first-principles", implying that physical constants are the only inputs into an *Ab initio* calculation. To further explain this term, according to computational many-body physics (Fehske et al., 2008), *Ab initio* is the term refers to a family of theoretical concepts and computational approaches that treat the many-electron problem from the beginning. Studying the electronic, optical and magnetic properties of a system are impossible at the empirical level due to these properties are highly dependent on an interplay of the spatial arrangement of the ions and the resulting distribution and density of electrons.

*Ab initio* computational methods, such as HF and DFT, are the common choice for solving correlated many-body problems which involve complex quantum mechanical contributions from the electronic degree of freedom in the system. In this thesis, calculations for the structural and electronic properties of the clusters are all done using DFT, which technical details are to be discussed in the following sections, starting from the fundamental Schrödinger equation to various approximations that lead to the modern DFT.

### 2.2.1 The Schrödinger Equation

DFT is a very useful quantum mechanical calculation scheme devised to investigate the ground-state electronic structure of a many-body system, e.g., a cluster of atoms. In solid-state physics and quantum chemistry, the ultimate objective of this *Ab initio* computational method is to calculate the electronic, optical and magnetic properties of a system as accurate as possible by solving the Schrödinger equation, given the chemical composition and the geometrical structure of the system. Given, the time-independent, non-relativistic Schrödinger equation with the eigenvalue  $E$ :

$$\hat{H}\Psi(\mathbf{r}_1, \mathbf{r}_2, \dots, \mathbf{r}_N, \mathbf{R}_1, \mathbf{R}_2, \dots, \mathbf{R}_M) = E\Psi(\mathbf{r}_1, \mathbf{r}_2, \dots, \mathbf{r}_N, \mathbf{R}_1, \mathbf{R}_2, \dots, \mathbf{R}_M), \quad (2.1)$$

where  $\Psi$  is the wave function of the atoms in a well-defined boundary region. In the following,  $\mathbf{R} = \{\mathbf{R}_1, \mathbf{R}_2, \dots, \mathbf{R}_M\}$  denotes the set of nucleus coordinates, and  $\mathbf{r} = \{\mathbf{r}_1, \mathbf{r}_2, \dots, \mathbf{r}_N\}$  the set of electron coordinates.

The Hamiltonian operator  $\hat{H}$  comprised of kinetic and potential energy terms. The latter describes the interaction between electron-electron, electron-nuclei and nuclei-nuclei.

The non-relativistic Hamiltonian  $\hat{H}$  for a molecule contains five terms,

$$\begin{aligned} \hat{H} = & \sum_{\alpha=1}^M -\frac{\hbar^2}{2M_\alpha} \nabla_\alpha^2 + \sum_{i=1}^N -\frac{\hbar^2}{2m} \nabla_i^2 - \sum_{i,\alpha=1}^{N,M} \frac{Z_\alpha e^2}{4\pi\epsilon_0 |\mathbf{r}_i - \mathbf{R}_\alpha|} \\ & + \frac{1}{2} \sum_{i \neq j}^N \frac{e^2}{4\pi\epsilon_0 |\mathbf{r}_i - \mathbf{r}_j|} + \frac{1}{2} \sum_{\alpha \neq \beta}^M \frac{Z_\alpha Z_\beta e^2}{4\pi\epsilon_0 |\mathbf{R}_\alpha - \mathbf{R}_\beta|}. \end{aligned} \quad (2.2)$$

The first two terms represent the kinetic energy term for the electrons and nuclei. The other three terms describe the electrostatic attraction between the  $N$  electrons and  $M$  nuclei, potential energy due to electron-electron interactions and nucleus-nucleus repulsions. In the atomic unit, the Hamiltonian  $\hat{H}$  is simplified to

$$\begin{aligned} \hat{H} = & \sum_{\alpha=1}^M -\frac{1}{2M_\alpha} \nabla_\alpha^2 + \sum_{i=1}^N -\frac{1}{2} \nabla_i^2 - \sum_{i,\alpha=1}^{N,M} \frac{Z_\alpha}{|\mathbf{r}_i - \mathbf{R}_\alpha|} \\ & + \frac{1}{2} \sum_{i \neq j}^N \frac{1}{|\mathbf{r}_i - \mathbf{r}_j|} + \frac{1}{2} \sum_{\alpha \neq \beta}^M \frac{Z_\alpha Z_\beta}{|\mathbf{R}_\alpha - \mathbf{R}_\beta|}. \end{aligned} \quad (2.3)$$

The operator for the kinetic energy to both electron and nucleus in an atomic system is given by

$$\nabla_i^2 = \left( \frac{\partial^2}{\partial r_{1i}^2} + \frac{\partial^2}{\partial r_{2i}^2} + \frac{\partial^2}{\partial r_{3i}^2} \right), \nabla_\alpha^2 = \left( \frac{\partial^2}{\partial R_{1\alpha}^2} + \frac{\partial^2}{\partial R_{2\alpha}^2} + \frac{\partial^2}{\partial R_{3\alpha}^2} \right). \quad (2.4)$$

The Hamiltonian  $\hat{H}$  can be written in a more compact form,

$$\hat{H} = \hat{T}_N(\mathbf{R}) + \hat{T}_e(\mathbf{r}) + \hat{V}_{Ne}(\mathbf{R}; \mathbf{r}) + \hat{V}_{ee}(\mathbf{r}) + \hat{V}_{NN}(\mathbf{R}), \quad (2.5)$$

The  $\hat{V}_{Ne}(\mathbf{R}; \mathbf{r})$  term contains degrees of freedom from both the nuclei and electrons that are coupled in a non-trivial manner. A Born-Oppenheimer approximation is introduced here to decouple the motions of the electron from that of the nuclear. The approximation allows one to solve the equations that describe the electron motion for atomic nuclei that are held fixed in space (namely,  $\mathbf{R}$ ). As a result of the Born approximation, the molecular wave function of the Hamiltonian then assumes the following form

$$\Psi(\mathbf{r}, \mathbf{R}) = \chi(\mathbf{R}) \cdot \psi(\mathbf{r}, \mathbf{R}). \quad (2.6)$$

The product of wave functions  $\chi(\mathbf{R})$  and  $\psi(\mathbf{r}, \mathbf{R})$  in Eq. (2.6) is also known as the Born-Oppenheimer wave function. The function  $\chi(\mathbf{R})$  is a vibrational function of the nuclear coordinates  $\mathbf{R}$ , whereas  $\psi(\mathbf{r}, \mathbf{R})$  is the electronic function of both nuclear coordinates  $\mathbf{R}$  and that of the electrons  $\mathbf{r}$ . In Eq. (2.6), the electronic wave function only depends on electronic coordinates  $\mathbf{r}$  with fixed parameters  $\mathbf{R}$ .

Subjected to the charge neutrality of an atom, the forces acting on both nucleus and electrons are equal but opposite. As a result, the changes in momentum due to these forces must be almost the same. Since the mass of the nuclei is much larger than the electrons, the nuclei move much slower than the electrons. As such, the kinetic energy of the nuclei  $\hat{T}_N(\mathbf{R})$  can be neglected from Eq. (2.5) as  $\hat{T}_N(\mathbf{R}) \ll \hat{T}_e(\mathbf{r})$ . The potential energy of nucleus-nucleus repulsion  $\hat{V}_{NN}(\mathbf{R})$  is just a constant and hence also neglected in Eq. (2.5). Thus, with the Born approximation, the electronic Hamiltonian is reduced to

$$\begin{aligned} \hat{H}_{elec} &= - \sum_{i=1}^N \frac{1}{2m} \nabla_i^2 - \sum_{i,\alpha=1}^{N,M} \frac{Z_\alpha}{|\mathbf{r}_i - \mathbf{R}_\alpha|} + \frac{1}{2} \sum_{i \neq j}^N \frac{1}{|\mathbf{r}_i - \mathbf{r}_j|} \\ &= \hat{T}_e(\mathbf{r}) + \hat{V}_{Ne}(\mathbf{R}; \mathbf{r}) + \hat{V}_{ee}(\mathbf{r}) \end{aligned} \quad (2.7)$$

$$\hat{V}_{Ne}(\mathbf{R}; \mathbf{r}) = V_{ext}(\mathbf{r}) = - \sum_{i,\alpha=1}^{N,M} \frac{Z_\alpha}{|\mathbf{r}_i - \mathbf{R}_\alpha|},$$

and Eq. (2.1) is reduced to

$$\hat{H}_{elec} \psi_{elec}(\mathbf{r}_1, \mathbf{r}_2, \dots, \mathbf{r}_N) = E_{elec} \psi_{elec}(\mathbf{r}_1, \mathbf{r}_2, \dots, \mathbf{r}_N). \quad (2.8)$$

Note that the potential energy due to the attraction of the  $N$  electrons by the  $M$  nucleus  $\hat{V}_{Ne}(\mathbf{R}; \mathbf{r})$  is also known as the external potential energy  $V_{ext}(\mathbf{r})$  in DFT. From Eq. (2.8), the minimal description of the Schrödinger equation, which ignores the contributions from the spins of electrons, is

$$\left( \hat{T}_e(\mathbf{r}) + \hat{V}_{ext}(\mathbf{r}) + \hat{V}_{ee}(\mathbf{r}) \right) \psi = E_{elec} \psi \quad (2.9)$$

In addition, the total energy  $E_{tot}$  is the sum of the  $E_{elec}$  and the constant nuclear repulsion term  $E_{nucl}$  (also known as nucleus repulsive energy),

$$E_{tot} = E_{elec} + E_{nucl} = E_{elec} + \frac{1}{2} \sum_{\alpha > \beta}^M \frac{Z_\alpha Z_\beta}{|\mathbf{R}_\alpha - \mathbf{R}_\beta|}. \quad (2.10)$$

### 2.2.2 Electron density

The many-body wave function contains all the possible information of a system that satisfies the requirement of the many-electron Schrödinger equation. However, the amount of information contained by the wave function is enormous, and its complexity is overwhelming; a  $3N$ -dimensional function (become  $4N$ -dimensional when the spin of an electron is considered). It turns out that the computational complexity caused by the many-body wave function can be alleviated by solving for the electron density instead of the wave function itself. The solution can be brought back to 3-dimensional space, as will be shown later.

In quantum mechanics, the electron density of a state is defined as the number of electrons per unit volume in a given state (Parr & Yang, 1989). Electron density is a

scalar quantity depending upon three spatial variables; most importantly, it is a measure of a probability of an electron occupying an infinitesimal element of space surrounding any given point  $\mathbf{r}$ . According to Born's statistical interpretation, the one-electron density for a system is defined as

$$n(\mathbf{r}) = |\psi(\mathbf{r})|^2, \quad (2.11)$$

absolute square of wave function. By using the conventional interpretation of observables from wave function, the expectation value of the electron density is written as

$$n(\mathbf{r}) = \langle \psi | \hat{n}(\mathbf{r}) | \psi \rangle = \int \psi^* \hat{n}(\mathbf{r}) \psi d\mathbf{r}, \quad (2.12)$$

where  $\hat{n}(\mathbf{r})$  is an operator corresponding to electron density. Here, electrons are considered as point particles, and the electron density is defined to be:

$$\hat{n}(\mathbf{r}) = \sum_{i=1}^N \delta(\mathbf{r}_i - \mathbf{r}), \quad (2.13)$$

where the Dirac delta function is used, and the position of the  $i$ -th electron is denoted  $\mathbf{r}_i$ . The operator  $\hat{n}(\mathbf{r})$  is the summation of all the density of electrons  $i$  at  $\mathbf{r}$  over the number of electrons.

Substitute Eq. (2.13) into Eq. (2.12), the expectation value of the electron density without electron spin, is then:

$$\begin{aligned} n(\mathbf{r}) &= \int \dots \int \psi^*(\mathbf{r}_1, \mathbf{r}_2, \dots, \mathbf{r}_N) \hat{n}(\mathbf{r}) \psi(\mathbf{r}_1, \mathbf{r}_2, \dots, \mathbf{r}_N) d\mathbf{r}_1, d\mathbf{r}_2 \dots d\mathbf{r}_N \\ &= \sum_{i=1}^N \int \dots \int \psi^*(\mathbf{r}_1, \mathbf{r}_2, \dots, \mathbf{r}_N) \delta(\mathbf{r}_i - \mathbf{r}) \psi(\mathbf{r}_1, \mathbf{r}_2, \dots, \mathbf{r}_N) d\mathbf{r}_1, d\mathbf{r}_2 \dots d\mathbf{r}_N \\ &= \sum_{i=1}^N \int \dots \int \psi^*(\mathbf{r}_1, \mathbf{r}_2, \dots, \mathbf{r}_N) \delta(\mathbf{r}_1 - \mathbf{r}) \psi(\mathbf{r}_1, \mathbf{r}_2, \dots, \mathbf{r}_N) d\mathbf{r}_1, d\mathbf{r}_2 \dots d\mathbf{r}_N \\ &= \sum_{i=1}^N \int \dots \int \psi^*(\mathbf{r}, \mathbf{r}_2, \dots, \mathbf{r}_N) \psi(\mathbf{r}, \mathbf{r}_2, \dots, \mathbf{r}_N) d\mathbf{r}_2 \dots d\mathbf{r}_N \\ &= N \int \dots \int |\psi(\mathbf{r}, \mathbf{r}_2, \dots, \mathbf{r}_N)|^2 d\mathbf{r}_2 \dots d\mathbf{r}_N. \end{aligned} \quad (2.14)$$

In the third line from the Eq. (2.14),  $\mathbf{r}_i$  is replaced by  $\mathbf{r}_1$  due to the consequences of Pauli's exclusion principle; all the electrons are identical and indistinguishable, and causing the probability  $|\psi(\mathbf{r}, \mathbf{r}_2, \dots, \mathbf{r}_N)|^2$  to be zero; hence an arbitrary electron must be selected to solve the Eq. (2.14). The existence of  $N$  represents the summation over all the identical electrons in the system. The preserved electron density overall space is ensured by the constant number of electrons  $N$ . From Eq. (2.14), the integral of the electron density gives the total number of electrons,

$$\int n(\mathbf{r}) d\mathbf{r} = N. \quad (2.15)$$

Typically, the wave function in Hartree Fock and DFT method is represented by single Slater determinant, constructed by orbital wave functions  $\varphi_i$ . Assume the spatial orbital is doubly filled, electron density from Eq. (2.14) can be simplified in terms of orbital wave functions:

$$n(\mathbf{r}) = 2 \sum_{i=1}^{\frac{N}{2}} |\varphi_i(\mathbf{r})|^2, \quad (2.16)$$

where the summation of the squares of the orbital wave functions is the density of electron at a point. The significance of factor 2 in Eq. (2.16) shows that the same orbital can be occupied by two electrons with a different spin, as stated by the Pauli exclusion principle.

### 2.2.3 Hohenberg-Kohn theorem

The iconic paper is written by Hohenberg and Kohn (Hohenberg & Kohn, 1964) as we know it today represents the major theoretical pillars on which all modern-day DFT are raised. The first theorem of Hohenberg-Kohn's work provides proof that the electron density is indeed physically justified.



**Hohenberg-Kohn first theorem:** *There is a unique ground state electron density  $n(\mathbf{r})$ , which employs to determine each of the external potential  $V_{ext}(\mathbf{r})$  in the system, within a trivial additive constant.*

Before the prove is given, at first, two external potential  $V_{ext}(\mathbf{r})$  and  $V'_{ext}(\mathbf{r})$  which differ more than a constant are considered, (which also means that  $V'_{ext}(\mathbf{r}) \neq V_{ext}(\mathbf{r}) + \text{const.}$ ). Assume that both wave functions  $\psi_0$  and  $\psi'$  give rise to the same electron density  $n_0(\mathbf{r})$ , and hence both external potential possess the same electron density  $n_0(\mathbf{r})$  associated with the corresponding non-degenerate ground states of  $N$  particles. These two potentials are parts of the two Hamiltonians (refer to Eq. (2.9)), which only differs in external potential can be expressed as  $\hat{H}_0 = \hat{T}_e(\mathbf{r}) + \hat{V}_{ext}(\mathbf{r}) + \hat{V}_{ee}(\mathbf{r})$  and  $\hat{H}' = \hat{T}_e(\mathbf{r}) + \hat{V}'_{ext}(\mathbf{r}) + \hat{V}_{ee}(\mathbf{r})$ . Obviously, Hamiltonians  $\hat{H}_0$  with a ground state wave function  $\psi_0$  and  $\hat{H}'$  with a ground state wave function  $\psi'$ , corresponding two different ground state energies,  $E_0$  and  $E'$  where  $E_0 \neq E'$ .

Since  $\psi$  is defined as a non-degenerate wave function, the application of the variational principle in which  $E$  is the minimal energy will lead to inequality:

$$\begin{aligned} E_0 < \langle \psi' | \hat{H} | \psi' \rangle &= \langle \psi' | \hat{H}' | \psi' \rangle + \langle \psi' | \hat{H}_0 - \hat{H}' | \psi' \rangle \\ E_0 < E' + \langle \psi' | \hat{V}_{ext}(\mathbf{r}) - \hat{V}'_{ext}(\mathbf{r}) | \psi' \rangle, \end{aligned} \quad (2.17)$$

which yields

$$E_0 < E' + \int n_0(\mathbf{r}) [\hat{V}_{ext}(\mathbf{r}) - \hat{V}'_{ext}(\mathbf{r})] d\mathbf{r}. \quad (2.18)$$

Interchanging the unprimed with the primed quantities and repeating the above steps of Eq. (2.18), the corresponding equation is expressed as

$$\begin{aligned} E' < \langle \psi_0 | \hat{H}' | \psi_0 \rangle &= \langle \psi_0 | \hat{H}_0 | \psi_0 \rangle - \langle \psi_0 | \hat{H}_0 - \hat{H}' | \psi_0 \rangle \\ E' < E_0 - \langle \psi_0 | \hat{V}_{ext}(\mathbf{r}) - \hat{V}'_{ext}(\mathbf{r}) | \psi_0 \rangle, \end{aligned} \quad (2.19)$$

which yields

$$E' < E_0 - \int n_0(\mathbf{r})[\hat{V}_{ext}(\mathbf{r}) - \hat{V}'_{ext}(\mathbf{r})] d\mathbf{r}. \quad (2.20)$$

Adding both Eqs. (2.18) and (2.20) give rises to the clear contradiction

$$E' + E < E + E' \text{ or } 0 < 0 \quad (2.21)$$

**Hohenberg-Kohn first theorem** conclusion: It is impossible for two external potential  $\hat{V}_{ext}(\mathbf{r})$  yield the identical ground state electron density; in other words, the external potential  $\hat{V}_{ext}(\mathbf{r})$  is uniquely specified by the corresponding ground state electron density.

The functional of the ground state electron density is represented the complete ground state energy and written as

$$E_0(n_0) = T(n_0) + V_{Ne}(n_0) + V_{ee}(n_0). \quad (2.22)$$

The functional of potential energy due to electrons and nuclei interactions depend on the actual system,  $V_{Ne}(n_0) = \int n_0(\mathbf{r}) V_{Ne}(n_0) d\mathbf{r}$ , and the rest energy functionals  $T(n_0)$  and  $V_{ee}(n_0)$  are independent parts, which defined as Hohenberg-Kohn functional  $F_{HK}(n_0)$ , where  $F_{HK}(n_0) = T(n_0) + V_{ee}(n_0)$ . Once again, the complete ground state energy can be expressed as

$$E_0(n_0) = F_{HK}(n_0) + \int n_0(\mathbf{r}) V_{Ne}(n_0) d\mathbf{r}. \quad (2.23)$$

**Hohenberg-Kohn second theorem:** *Electron density  $n$  defines a universal functional for the energy  $E(n)$ . The global minimum value of the overall functional is the exact ground state density,  $n_0$ .*

This theorem states that the ground state energy of the system can be delivered by the Hohenberg-Kohn functional  $F_{HK}(n_0)$ . Proving this theorem is very straightforward by the application of the variational principle. By variational principle,

$$\langle \psi' | \hat{H} | \psi' \rangle \geq \langle \psi_0 | \hat{H}_0 | \psi_0 \rangle \quad (2.24)$$

$$F_{HK}(n) + \int n(\mathbf{r}) V_{ext}(n) d\mathbf{r} \geq F_{HK}(n_0) + \int n_0(\mathbf{r}) V_{ext}(n_0) d\mathbf{r}$$

$$E_v(n) \geq E_v(n_0) = E_0,$$

the subscript  $v$  denotes energy that is related to the external potential.

**Hohenberg-Kohn second theorem** conclusion: External potential  $\hat{V}_{ext}(\mathbf{r})$  that used to determine all the properties of a system are determined by ground state density. Functional  $F_{HK}(n) + \int n(\mathbf{r}) V_{ext}(\mathbf{r}) d\mathbf{r}$  possesses the ground state energy with density  $n$ .

The minimum principle for the energy functional concerning electron density is well established by Hohenberg-Kohn second theorem. Especially, energy functional  $E_0(n_0)$  (refer Eq. (2.22)) require to be minimized with the underlying constraint of a constant number of electrons from the integration of electron density,  $\int n(\mathbf{r}) d\mathbf{r} = N$  (refer Eq. (2.15) ). Such constraint can be incorporated into the scheme via the well-known method of Lagrange multipliers. In this method, the constrained Langrangian

$$L_{v,N} = E_v(n) - \mu \left[ \int n(\mathbf{r}) d\mathbf{r} - N \right], \quad (2.25)$$

is minimized with respect to the electron density as per

$$\frac{\delta L_{v,N}}{\delta n(\mathbf{r})} = \frac{\delta [F_{HK}(n) + \int n(\mathbf{r}) V_{ext}(\mathbf{r}) d\mathbf{r} - \mu [\int n(\mathbf{r}) d\mathbf{r} - N]]}{\delta n(\mathbf{r})} = 0$$

$$\mu = \frac{\delta [F_{HK}(n)]}{\delta n(\mathbf{r})} + V_{ext}(\mathbf{r}) = 0. \quad (2.26)$$

This is the basic equation for DFT.

#### 2.2.4 Kohn-Sham formalism

Although the complexity and dimensionality of many-body Schrödinger equation are reduced drastically by Hohenberg and Kohn (1964), however, they do not